This is the author's peer reviewed, accepted manuscript. However, the online version of record will be different from this version once it has been copyedited and typeset

PLEASE CITE THIS ARTICLE AS DOI: 10.1063/5.0090041

### Localization in inhomogeneously broadened systems using the Gibbs phenomenon

Zhaoyuan Gong<sup>1</sup> and Jamie D. Walls<sup>1</sup> Department of Chemistry, University of Miami, Coral Gables, Florida 33146,USA

(\*Electronic mail: jwalls@miami.edu)

(Dated: 5 May 2022)

Spectra and images derived from the Fourier transformation of time-domain signals can often exhibit overshoots and/or "ringing" near sharp features. Such artifacts are due to the slow convergence of the Fourier series near such features, an effect referred to as the Gibbs phenomenon. While usually viewed as being purely mathematical in origin, the Gibbs phenomenon can often be found in a variety of physical situations, such as in imaging and spectroscopy. In this work, a physical description of the Gibbs phenomenon is presented where it is interpreted as an interference effect whereby slower destructive interference or "Fourier dephasing" occurs near sharp spectral features compared with the Fourier dephasing observed away from such features. Such differences in Fourier dephasing can be exploited to localize magnetization near physical boundaries on timescales about an order of magnitude faster than can be achieved using conventional frequency or spatially selective pulses. This localization, which is reversible, also occurs on much faster timescales than can be attributed to irreversible sources such as restricted diffusion or spatial variations of the intrinsic spin relaxation within the sample.

Ever since Joseph Fourier introduced the (then) revolutionary concept that functions could be represented by a series of sines and cosines, applications of Fourier series by scientists and engineers to transform experimental data into interestable forms, such as spectra or images, have become commonplace. While most applications require finding Fourier series representing smooth or infinitely differentiable functions, the Fourier series of non-smooth functions can often exhibit oscillations and/or overshoots at frequencies where the function is not infinitely differentiable. This effect, which is referred to as the Gibbs phenomenon<sup>1,2</sup>, is the result of representing a function that is not smooth at a finite number of frequencies in terms of basis functions that are themselves smooth over the entire frequency range, e.g., the sine and cosine basis functions of a Fourier series. The Gibbs phenomenon can often be observed in signal processing applications when sharp filters are applied to time-domain signals, and it was also recently observed in numerical studies of electron transport due to filtering the calculated current over a finite bandwidth<sup>3</sup>. In imaging and spectroscopic applications, the Gibbs phenomenon often arises as a result of truncating signal acquisition in time<sup>4</sup>. A Gibbs overshoot and/or "ringing" artifact often occurs near such sharp spectral features, which need higher frequencies in order to accurately depict them, due to insufficient signal acquisition times.

Recently, spectral localization near boundaries observed in nuclear magnetic resonance (NMR) delayed-acquisition experiments [pulse sequence in Fig. 1(A)] was also attributed to the Gibbs phenomenon<sup>6</sup>. As illustrated in Fig. 1(B), a magnetic field gradient of strength g applied along the length of a Shigemi tube, which has a flat bottom, causes each "XY-slice" within the sample to resonate at a slightly different frequency along the  $\hat{z}$ -direction,  $\omega(z) = \gamma gz$ , where  $\gamma$  is the gyromagnetic ratio, and  $z = |\mathbf{z}|$  is the z-coordinate along the axis of the tube. In Fig. 1(B), the Gibbs phenomenon was observed for signals near the bottom edge of the Shigemi tube (taken to be at z = 0 mm) due to insufficient signal acquisition in time. When an acquisition delay of  $T_{\text{Delay}} = 1$  was applied,

signal was localized near the bottom edge of the Shigemi tube as shown in Fig. 1(C). In an NMR context, it is known that an acquisition delay results in larger signal attenuation for spins with short transverse relaxation or  $T_2^*$  times, leaving only long-lived signals that result in narrower spectra. From the delayed-acquisition spectra in Fig. 1(C), the magnetization near the bottom edge has a longer effective  $T_2^*$  time compared to the magnetization within bulk.

Why signals near edges have longer apparent  $T_2^*$  times can be partially understood within a magnetic resonance imaging (MRI) context. In MRI, it is known that delayedacquisition simply filters out low spatial frequencies, i.e., low values in k-space, leaving only higher k-space values. Since edges/boundaries are characterized by higher spatial frequencies, an image reconstructed with only high k-space values will highlight the edges/boundaries<sup>8</sup>, which is generally interpreted as being an image processing effect and not a physical effect due to magnetization actually being localized near physical edges/boundaries. To reconcile both the NMR and MRI pictures of signal localization near edges under delayedacquisition, it was argued<sup>6</sup> that the slow signal decay near edges was due to the slow convergence of the Fourier series needed to describe a system with a magnetization density having sharp edges, i.e, signal localization was due to the Gibbs phenomenon.

While the above argument provided a mathematical description behind the physical localization of transverse magnetization observed in Fig. 1, no *physical* mechanism was presented that described how the Gibbs phenomenon led to such spectral localization. In this work, the Gibbs phenomenon is physically interpreted as an interference effect. Magnetization near sharp features, such as boundaries or edges, experience slower destructive interference or "Fourier dephasing" relative to the magnetization found within the bulk. As a result of this difference in Fourier dephasing, reversible spectral/spatial localization of transverse magnetization in the presence of a magnetic field gradient occurs near boundaries. Furthermore, it is experimentally demonstrated that this localization occurs

This is the author's peer reviewed, accepted manuscript. However, the online version of record will be different from this version once it has been copyedited and typeset

PLEASE CITE THIS ARTICLE AS DOI: 10.1063/5.0090041

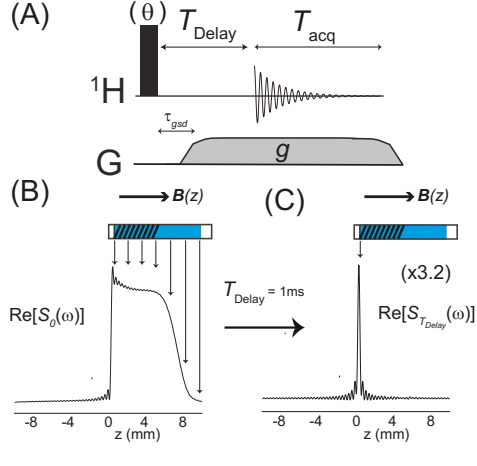


FIG. 1. (A) Basic delayed-acquisition NMR sequence. After an initial excitation pulse of flip-angle  $\theta$ , a gradient of strength g is turned on with a gradient stabilization delay of  $\tau_{gsd} = 110 \,\mu s$ . Following an acquisition delay of T<sub>Delay</sub> after an initial excitation pulse, the FID is acquired at integer multiples of the dwell time,  $\Delta t$ , for a time  $T_{\text{acq}} = N_{\text{pts}} \Delta t$ . (B) Real part of the spectrum, Re $[S_0(\omega)]$ , for a 10:90 (v/v) H2O/D2O solution in a D2O susceptibility matched Shigemi tube [the schematic of a Shigemi tube with a magnetic field and linear field gradient applied perpendicular to the Shigemi tube's bottom edge located at z = 0,  $\mathbf{B}(\mathbf{z}) = \mathbf{B}_0 + g\mathbf{z}$  with g = 2.96 gauss/cm. The main sample detection region was approximately 5 mm (shown in the schematic) with signals attenuated outside this region ( $z \ge 5$  mm)]. The FID was acquired using the sequence in (A) with  $T_{Delay} = 0$  and  $T_{\rm acq} = 4096\Delta t$ , although only the first 96 complex points were transformed using a discrete Fourier transform (DFT), which resulted in a Gibbs overshoot and ringing artifact in the spectrum near the bottom of the Shigemi tube ( $z \approx 0$  mm). (C) With  $T_{\text{Delay}} = 1$  ms, signal was predominantly localized near the bottom tube edge. The delayed-acquisition spectrum was scaled by a factor of  $(\times 3.2)$  for better comparison to the image in (B). It should also be noted that the purpose of D2O in the sample was simply to dilute the water magnetization in order to reduce the effects of radiation damping<sup>5</sup> All experiments in this work were performed on a 400 MHz Bruker AVANCE III HD spectrometer with a Micro5 microimaging probe equipped with XYZ gradients and a <sup>1</sup>H channel. The spectra in (B) and (C) were acquired using Bruker TopSpin, a relaxation delay of 20 s, a dwell time of  $\Delta t = 25 \mu$ s, and  $N_S = 8$  scans.

on a faster timescale than can be attributed to irreversible localization mechanisms such as restricted diffusion<sup>9,10</sup>

For a system with a magnetization density  $\rho(\mathbf{r})$ , the evolution of the transverse magnetization generated by an initial  $\theta$ -excitation and in the presence of an applied magnetic field gradient [sequence in Fig. 1(A) with  $T_{Delay} = 0$ ]. This signal, which is referred to as the free induction decay (FID), is sampled at integer multiples of the dwell time,  $n\Delta t$  for n = 0 to  $n = N_{\rm pts} - 1$ , and can be calculated by (in the absence of  $T_2^*$ 

relaxation and diffusion):

FID
$$(t = n\Delta t) = \langle M_{+}(t) \rangle = \sin(\theta) \int dr^{3} \rho(\mathbf{r}) e^{-i\gamma \mathbf{g} \cdot \mathbf{r} t}$$
  

$$= \sin(\theta) \int_{-L}^{L} dz' \rho_{Z}(z') e^{-i\gamma gz' t}$$
  

$$= \sin(\theta) (1 + \delta_{n0}) \frac{\pi}{\Delta t} (A_{n} + iB_{n})$$
(1)

where  $\rho_Z(z)=\int \mathrm{d}x'\mathrm{d}y' \rho(z,x',y')$  and  $2L=\frac{2\pi}{\gamma g \Delta t}$  are the effective one-dimensional magnetization density and field of view (FOV), respectively, along the gradient direction (taken to be the  $\widehat{z}$ -direction),  $\delta_{kj}$  is the Kronecker delta function, and  $A_n$ and  $B_n$  are the  $n^{th}$  coefficients in the Fourier series of  $\rho_Z(z)$ :

$$\rho_Z(z) = A_0 + \sum_{n=1}^{\infty} A_n \cos\left(\frac{\pi nz}{L}\right) + B_n \sin\left(\frac{\pi nz}{L}\right)$$
 (2)

Consider a  $\rho_Z(z)$  that is uniformly distributed between  $z=\pm L_0,\, \rho_Z(z)=\frac{1}{2L_0}$  for  $|z|\leq L_0$  and  $\rho_Z(z)=0$  for  $L_0<|z|< L$ . For such a  $\rho_Z(z)$ ,  $A_0 = \frac{1}{2L}$ ,  $B_n = 0$ , and  $A_n = \frac{1}{L} \operatorname{sinc} \left( \frac{n\pi L_0}{L} \right)$ . The spectrum with  $T_{\text{Delay}} = 0$ ,  $S_0(\omega)$ , is obtained by applying a discrete Fourier transform (DFT) to the FID(t) in Eq. (1) and is given by (for  $|\omega| \le \gamma gL$ ):

$$S_0(\omega) = \frac{\pi \sin(\theta)}{2\Delta t L} \left( 1 + 2 \sum_{n=1}^{N_{\text{pts}} - 1} \text{sinc}\left(\frac{n\pi L_0}{L}\right) e^{in\omega \Delta t} \right) (3)$$

Note that  $\text{Re}[S_0(\omega)]$  approximates  $\rho_Z(z)$  where the sum in Eq. (2) only includes the first  $N_{\rm pts}$  Fourier coefficients. In this case,  $Re[S_0(\omega)]$  will exhibit a Gibbs overshoot near  $\omega \pm \gamma G L_0$ . For an acquisition delay of  $T_{\text{Delay}} = N_D \Delta t$ , the corresponding spectrum<sup>6</sup>,  $S_{T_{Delay}}(\omega)$ , is given by:

$$\begin{split} S_{T_{\text{Delay}}}(\omega) &= \frac{\pi \sin(\theta)}{\Delta t L} \text{sinc}\left(\frac{N_D \pi L_0}{L}\right) \\ &+ \frac{\pi \sin(\theta)}{\Delta t L} \sum_{k=1}^{N_{\text{pts}}-1} \text{sinc}\left(\frac{(N_D + k) \pi L_0}{L}\right) e^{i\omega k \Delta t} (4) \end{split}$$

In this case,  $|S_{T_{\rm Delay}}(\omega)|$  will be concentrated near  $\omega \approx \pm \gamma G L_0$ , similar to what was observed in Fig. 1(C); however, it is not clear from Eq. (4) why that should be the case.

To gain some insight into the localization of magnetization near  $\omega = \pm \gamma G L_0$ , consider approximating  $\rho_Z(z)$  by the

$$\rho_{Z}(z) \approx \rho_{Z,N}(z) = \frac{1}{2L_0} \left( \frac{1}{\left(\frac{z}{L_0}\right)^{2n} + 1} \right)$$
 (5)

for  $N\gg 1$ . In the limit  $N\to\infty$ ,  $\rho_{Z,\infty}(z)$  approaches the uniform distribution described above. Using  $\rho_{Z,N}(z)$ , the FID(t) in Eq. (1) is given by:

$$\begin{aligned} \text{FID}(t) &= \frac{\sin(\theta)}{2L_0} \int_{-L}^{L} \mathrm{d}z' \frac{e^{-i\gamma Gtz'}}{\left(\frac{z'}{L_0}\right)^{2N} + 1} \approx \frac{\sin(\theta)}{2} \int_{-\infty}^{\infty} \mathrm{d}z' \frac{e^{-i\gamma GtL_0z'}}{(z')^{2N} + 1} \\ &= \frac{i\pi \sin(\theta)}{N} \sum_{m=0}^{N-1} \lambda_m e^{-(\Gamma_m + i\omega_m)t} \end{aligned} \tag{6}$$

where  $\lambda_m = \exp\left(-i\frac{\pi(2m+1)}{2N}\right)$  for m = 0 to m = N - 1 are the 2N roots of "-1" (i.e.,  $(\lambda_m)^{2N} = -1$ ) in the lower half of the complex plane, and  $\Gamma_m = \gamma G L_0 \sin\left(\frac{\pi(2m+1)}{2N}\right)$  and  $\omega_m =$  $\gamma GL_0\cos\left(rac{\pi(2m+1)}{2N}
ight)$  are the effective  $T_2^*$  and frequency of the  $m^{th}$  exponential in Eq. (6). Note that in the limit  $N \to \infty$ ,  $FID(t) \rightarrow sinc(\gamma GL_0t)$  as expected for transverse magnetization uniformly distributed between  $-L_0 \le z \le L_0$  (see Supplementary Material (SM) for more details).

Since the FID(t) in Eq. (6) is simply the sum of N frequency-shifted, exponential decays in time, the resulting spectrum will consist of N, frequency shifted lorentzians with the  $k^{th}$  lorentzian centered about  $\omega_k$  with a linewidth of  $\Delta v_{\frac{1}{2},k} = \frac{\Gamma_k}{\pi}$ . An example of this is given in Fig. 2 for  $\rho_{Z,900}(z)$ in Eq. (5) and for  $T_{\rm acq} = \frac{400\pi}{\gamma GL_0}$ . In the absence of an acquisition delay  $(T_{\rm Delay} = 0)$ , Real  $[S_0(\omega)]$  in Fig. 2(A) was uniformly distributed between  $\omega = \pm \gamma G L_0$ . A small, Gibbs ringing artifact observable at  $\omega \approx \pm \gamma G L_0$  was due to the short  $T_{\rm acq}$  used in the calculation (for  $T_{\rm acq} \ge \frac{900\pi}{\gamma GL_0}$ , no oscillations were observed in the calculations since  $\rho_{Z,N}(z)$  is a smooth function for finite N). The contributions to Real  $[S_0(\omega)]$  for a few lorentzians (m = 1, 25, 250 and 450) are also shown in Fig. 2(A). As expected from Eq. (6), the individual spectra near the edge (m = 1 and m = 25) were narrower and antiphase (i.e., phase shifted by  $\approx -\frac{\pi}{2}$  since  $\lambda_1 \approx \lambda_{25} \approx e^{\frac{-i\pi}{2}}$ ), which contributed to the Gibbs ringing artifact at the edges of Real  $[S_0(\omega)]$  in Fig. 2(A). The individual spectra near the middle of the distribution (m = 250 and m = 450) were more in-phase  $(\lambda_m \approx 1)$  and were much broader due to larger  $\Gamma_m$ . With an acquisition delay, the lorentzians were weighted by the factor  $S_n = \lambda_m e^{-(\Gamma_n + i\omega_n)}$  with  $|S_m| < 1$ . Since  $\Gamma_m$  is much larger for signals in the middle than for signals near the edges, the magnetization in the middle was more severely attenuated relative to the magnetization near the edges. For example, the middle signals (m = 250 and m = 450) were exponentially attenuated due to "Fourier dephasing" by a factor of  $|S_m| \approx 10^{-5} - 10^{-6}$  for a delay of  $T_{\text{Delay}} = \frac{4.5\pi}{\gamma GL_0}$ , while the signals near the edges were only attenuated by a factor of  $|S_m| \approx \frac{1}{2}$ , thereby resulting in spectral localization near  $\omega \approx \pm \gamma G L_0$  as shown in Fig. 2(B). Unlike true  $T_2$ -weighting, however, "Fourier-dephasing" is reversible, which can be exploited to improve the signal to noise (S/N) ratio of the edge signal as demonstrated in SM.

While Fig. 1 was consistent with reduced Fourier dephasing at the bottom edge of the Shigemi tube, it has long been appreciated in both classical and quantum systems that the dynamics near boundaries can be markedly different from that found within the bulk, and as such, alternative physical mechanisms behind the observed localization also need to be addressed. One such physical mechanism is restricted diffusion<sup>9</sup>. In the presence of a magnetic field gradient, magnetization is irreversibly attenuated due to diffusion<sup>11</sup>, decaying exponentially with increased mean square displacement. Reflections from physical boundaries, such as a container wall, however, can reduce the effective mean square displacement normal to the boundary surface relative to the

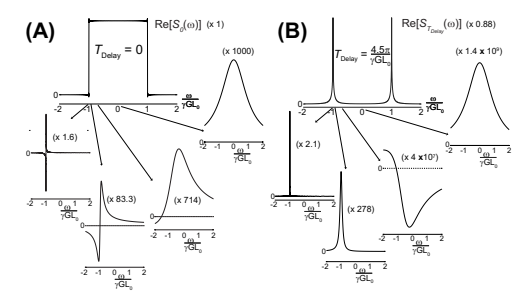


FIG. 2. (A) Numerical calculations of Real  $[S_0(\omega)]$  for a uniform distribution  $[\rho_{Z,900}(z)]$  in Eq. (5) in Eq. (5) along with the contributions from four individual lorentzians (from left to right, m=1, m=25, m=250, and m=450) for  $T_{\rm acq}=\frac{400\pi}{7GL_0}$ . (B) With  $T_{\rm Delay}=\frac{4.5\pi}{7GL_0}$ Real  $[S_{T_{\text{Delay}}}(\omega)]$  became localized near  $\omega \approx \pm \gamma GL_0$  due to slower "Fourier dephasing" at the edges. Spectral scaling factors are given in the figures and are denoted by (x number) so that the spectra are all plotted on the scale as Real  $[S_0(\omega)]$  in (A).

mean-square displacement found within the bulk. Such a reduction in mean square displacement due to reflections from boundaries is referred to as restricted diffusion 9,10,12-15. Due to restricted diffusion, magnetization appears to be localized at boundaries perpendicular to the applied gradient.

To experimentally assess the effects of restricted diffusion on the observed localization shown in Fig. 1, diffusionweighted, one-dimensional spectra were acquired and are shown in Fig. 3(A). In the diffusion-weighted sequence, dephasing under an applied gradient is partially refocused at a time  $\tau_{\Lambda}$  prior to acquisition due to the application of a  $\pi$ -pulse while allowing for both diffusion and (to a lesser extent)  $T_2$ relaxation to irreversibly attenuate the transverse magnetization. In Fig. 3(A), signal near the bottom edge ( $z \approx 0$  mm) became highlighted relative to the bulk signal for  $\tau_{\Delta} > 60$  ms, which was over an order of magnitude longer than the  $T_{\text{Delay}}$ needed to achieve similar localization in the corresponding delayed-acquisition experiment given in Fig. 3(B). Numerical simulations of the Bloch-Torrey equations also suggest that restricted diffusion is not necessary to explain the observed localization [See SM]. Taken in total, the results in Fig. 3 suggest that restricted diffusion is not responsible for the observed localization seen in Fig. 1. Furthermore, T<sub>2</sub>-maps indicated that differences in  $T_2$  relaxation times within the sample were also too small to account for the observed signal localization on the millisecond timescale observed in Fig. 1 and Fig. 3(B).

Differences in "Fourier dephasing" can be exploited to localize signals near boundaries by an order of magnitude faster than can be achieved using conventional selective pulses1 that satisfy the usual Fourier inequality for selective pulses,  $\Delta v_{\frac{1}{2}} T_p \ge 1$  where  $T_p$  is the selective pulse length<sup>20</sup>. In Fig. 4, a comparison of the XZ and XY images obtained from [Fig. 4(C)] a delayed-acquisition experiment ( $T_{\text{Delay}} = 1 \text{ ms}$ ) and those obtained using [Fig. 4(D)] "slice" selective pulses are



### **Applied Physics Letters**

This is the author's peer reviewed, accepted manuscript. However, the online version of record will be different from this version once it has been copyedited and typeset



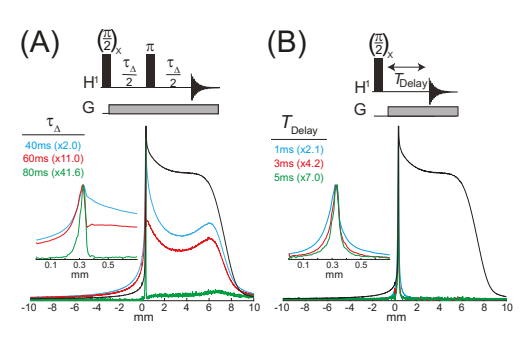


FIG. 3. Effects of restricted diffusion on signal localization. (A) Diffusion-weighted sequence and experimental spectra for a 10-90 (v/v)  $\text{H}_2\text{O}/\text{D}_2\text{O}$  in a Shigemi tube (same parameters as used in Fig. 1 with the exception that all spectra were processed using all 4096 complex points). Diffusion delays,  $\tau_\Delta$ , b values  $\left[b=\gamma^2G^2\frac{2}{3}\left(\frac{\tau_\Delta}{2}\right)^3\right]$ , and the corresponding attenuation factors due to diffusion,  $e^{-bD}$ , were: (blue)  $\tau_\Delta=40$  ms,  $b=3.3\times10^4\frac{s}{cm^2}$  and  $e^{-bD}=0.51$ , (red)  $\tau_\Delta=60$  ms,  $b=1.1\times10^5\frac{s}{cm^2}$  and  $e^{-bD}=0.10$ , and (green)  $\tau_\Delta=80$  ms,  $b=2.7\times10^5\frac{s}{cm^2}$  and  $e^{-bD}=4.7\times10^{-3}$ . Attenuation factors due to  $T_2$  relaxation were negligible since  $e^{-\frac{\tau_\Delta}{2}}=0.95-0.97$ . Compared to the (black)  $\frac{\pi}{2}$ -acquire spectrum, the edge signal was only localized for  $\tau_\Delta>60$  ms. (B) Delayed-acquisition experiments exhibited edge localization within milliseconds, narrowing with increasing  $T_{\text{Delay}}$ . Spectral scaling factors relative to the (black)  $\frac{\pi}{2}$ -acquire spectra are provided in all cases.

shown. Using a  $T_p = 12$  ms rectangular excitation pulse [Fig. 4(D), bottom] provided around 50% more signal compared to a delayed-acquisition experiment [Fig. 4(C)], while using a  $T_p = 40 \text{ ms Shinnar-Le-Roux (SLR) excitation pulse}^{17,18} \text{ gen-}$ erated a "cleaner" excitation slice near the bottom edge compared to the rectangular selective pulse [Fig. 4(D), top] although it also resulted in the worst S/N due to diffusion and  $T_2$ spin relaxation that occurred due to the long pulse length. For delayed-acquisition, the signal was localized along the bottom edge of the Shigemi tube, with a maximum of  $\Delta v_{\underline{1}} = 75$ Hz observed near the center of the bottom edge, whereas  $\Delta v_1 \approx 125$  for both slice selective excitation pulses. Treating the initial excitation and delay as an effective pulse of length  $T_p \approx T_{\text{Delay}} = 1$  ms in Fig. 4(C), the corresponding selective pulse Fourier inequality for delayed-acquisition was  $\Delta v_{\frac{1}{2}}T_p=0.075$ , which was over an order of magnitude smaller than  $\Delta v_{\frac{1}{8}}T_p$  obtained for conventional selective pulses  $(\Delta v_{\frac{1}{3}}T_p \approx 1.5 \text{ and } \Delta v_{\frac{1}{3}}T_p = 5 \text{ for the rectangular and SLR ex-}$ citation pulses, respectively).

While differences in Fourier dephasing can be exploited to localize signals, the question remains as to what is the minimum  $\Delta v_{\frac{1}{2}}$  that can be achieved due to Fourier dephasing? For  $\rho_{Z,\infty}(z)$ , the ultimate resolution is determined by the total acquisition time after the initial excitation pulse,  $T_{\rm acq}$ , which, due to S/N considerations, is typically fixed to be a few multi-

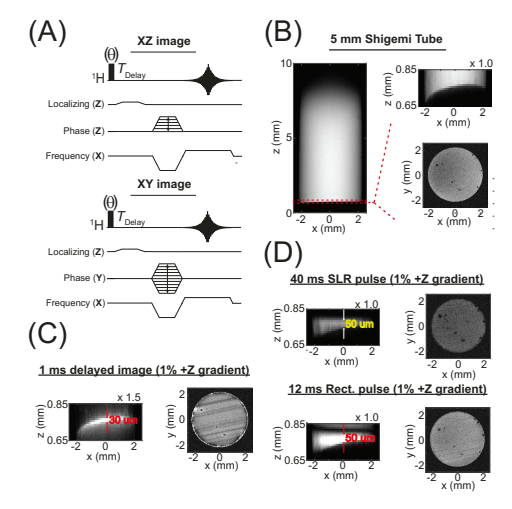


FIG. 4. Comparison of signal localization under delayed-acquisition and slice selective pulses. (A) Modified FLASH  $^{16}$  sequences to measure the (top) XZ and (bottom) XY-slices under delayed-acquisition. (B) XZ and XY images of a 10:90 (v/v)  $\rm H_2O/D_2O$  in a Shigemi tube with  $T_{\rm Delay}=0$ , an echo time of TE=3.2 ms, and a  $10\mu s$   $\theta=\frac{\pi}{6}$  excitation pulse. (C) XZ and XY images using TE=3.2 ms,  $T_{\rm Delay}=1$  ms, and  $\theta=\frac{\pi}{6}$ , which exhibited signal localization at the bottom edge of the Shigemi tube. (D) The hard  $\theta$ -pulse and  $T_{\rm Delay}$  in the imaging sequences in (A) were replaced by a slice selective pulse (top: 40ms Shinnar-Le-Roux pulse  $^{17.18}$  with TE=26.1 ms; bottom: 12ms rectangular pulse with TE=12.6 ms). The images were acquired using Paravision 6 with the following parameters: 250 ms repetition time,  $N_S=8$ , FOV = 5mm × 20mm with a matrix size of 512 × 2048 for the XZ images and a FOV = 5 mm × 5 mm with a matrix size of 512 × 512 for the XY images.

ples of the intrinsic  $T_2$ . So while increasing  $T_{\mathrm{Delay}}$  will lead to better signal localization at boundaries, increasing  $T_{\mathrm{Delay}}$  will also lead to a shorter, effective acquisition time,  $T_{\mathrm{acq}} - T_{\mathrm{Delay}}$ , which will lead to a "digital" broadening of the signal. As such, there will be an optimal  $T_{\mathrm{Delay}}^{\mathrm{optimal}}$  for a given  $T_{\mathrm{acq}}$  that minimizes  $\Delta v_{\frac{1}{2}}$ . For  $\rho_{Z,\infty}(z)$ , it was found from numerical simulations that the minimum  $\Delta v_{\frac{1}{2}}$  at the edges under delayed-acquisition and with  $T_{\mathrm{Delay}} > \frac{2\pi}{\gamma GL_0}$  occurred at:

$$T_{\mathrm{Delay}}^{\mathrm{optimal}} \approx (0.093 \pm 0.004) T_{\mathrm{acq}}$$
 (7)

corresponding to a line width of:

$$\Delta v_{\frac{1}{2}}^{\text{optimal}} = \frac{1.50 \pm 0.02}{T_{\text{acq}}}$$
 (8)

In conclusion, we have demonstrated that spectral localization can occur near sharp edges on a faster timescale than can be accounted for by physical mechanisms such as restricted diffusion and/or differences in intrinsic spin relaxation within a sample. The observed localization under an applied gradient



PLEASE CITE THIS ARTICLE AS DOI: 10.1063/5.0090041

was shown to be an interference effect related to the Gibbs phenomenon whereby slower destructive interference or Fourier dephasing occurred near edges/boundaries relative to that found within the bulk. Such effects could possibly be exploited in the development of new spatially selective pulses that incorporate Fourier dephasing in their design in order to achieve faster signal localization compared to conventional spatially selective pulses. Since the interference effects discussed in this work are general, its possible that they could have an effect on electron interference phenomenon observed in mesoscopic systems. For example, Fourier dephasing may have some bearing on recent theoretical work on quantum scarring<sup>21,22</sup>.

### SUPPLEMENTARY MATERIAL

Additional mathematical details and calculations of the spectrum using  $\rho_{Z,n}(z)$  in Eq. (5) are presented, numerical studies of the effects of diffusion, and additional experimental MRI results on signal localization.

### **ACKNOWLEDGMENTS**

We would like to acknowledge support from the National Science Foundation under CHE - 1056846, CHE - 1626015, and CHE - 1807724 and discussions with Dr. Ryan Berndt (Otterbein College).

### DATA AVAILABILITY STATEMENT

The data that support the findings of this study are available from the corresponding author upon reasonable request.

- <sup>1</sup>J. W. Gibbs, "Fourier's series," Nature **59**, 200 (1898).
- <sup>2</sup>J. W. Gibbs, "Fourier's series," Nature **59**, 606 (1899).

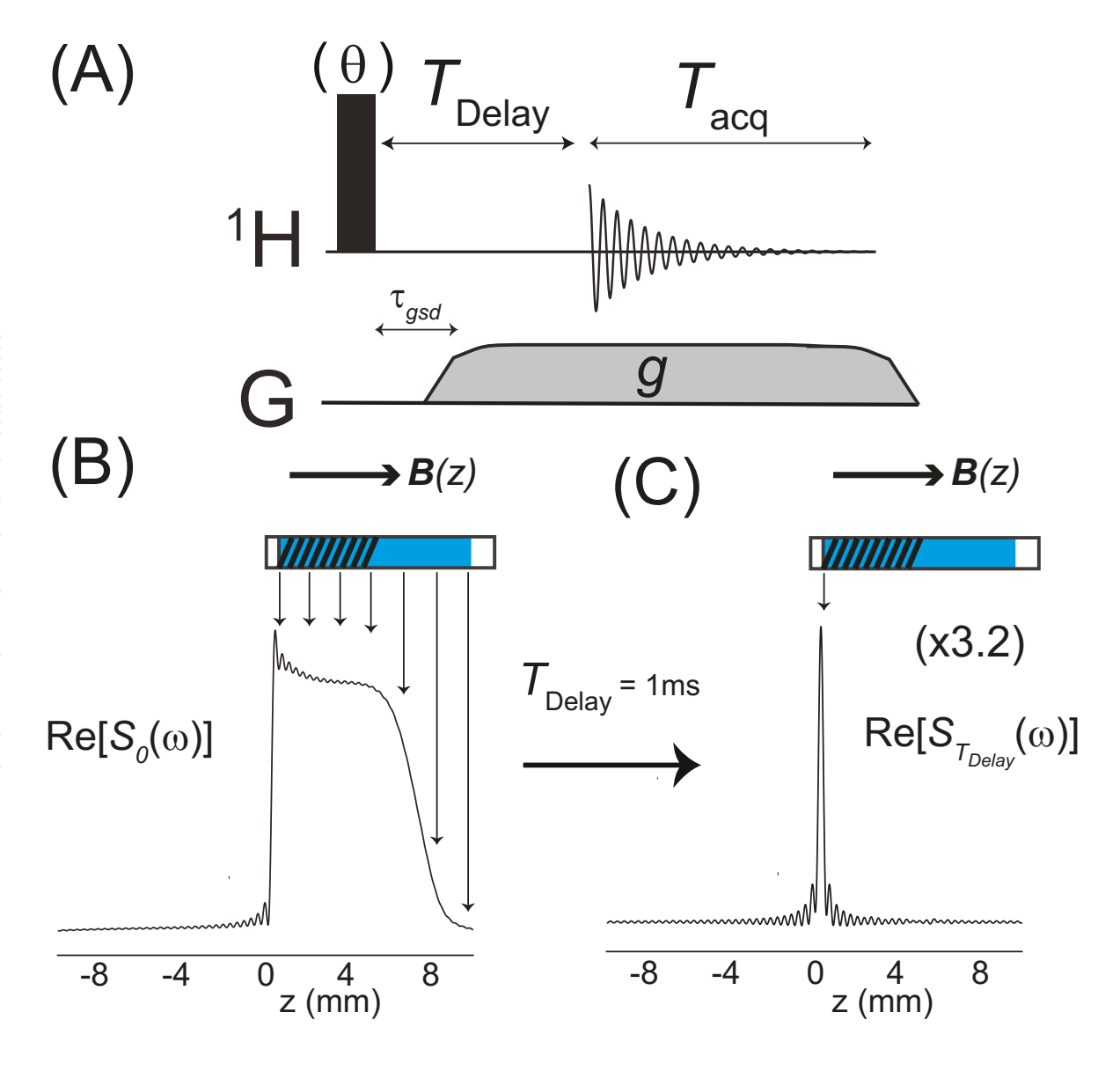
  <sup>3</sup>M. Zwolak, "Communication: Gibbs phenomenon and the emergence of the steady-state in quantum transport," J. Chem. Phys. 149, 241102 (2018).

- <sup>4</sup>E. Kellner, B. Dhital, V. G. Kiseley, and M. Reisert, "Gibbs-ringing artifact removal based on local subvoxel-shifts," Mag. Res. Med. 76, 1574-1581
- <sup>5</sup>W. S. Warren, S. L. Hammes, and J. L. Bates, "Dynamics of radiation damping in nuclear magnetic resonance," J. Chem. Phys. 91, 5895–5904
- <sup>6</sup>Z. Gong and J. D. Walls, "Enhancing the detection of edges and nondifferentiable points in an NMR spectrum using delayed-acquisition." J. Mag. Res. 287, 15–24 (2018).
- <sup>7</sup>C. H. A. Seiter, G. W. Feigenson, S. I. Chan, and M.-C. Hsu, "Delayed fourier transform proton magnetic resonance spectroscopy," J. Am. Chem. Soc. **94**, 2535–2537 (1972).
- R. Mezrich, "A perspective on k-space," Radiology 195, 297–315 (1995).
   S. D. Stoller, W. Happer, and F. J. Dyson, "Transverse spin relaxation in inhomogeneous magnetic fields," Phys. Rev. A 44, 7459-7477 (1991).
- <sup>10</sup>N. Moutal and D. S. Grebenkov, "The localization regime in a nutshell," J.
- Mag. Res.  $\bf 320$ , 106836 (2020).  $^{11}$  H. C. Torrey, "Bloch equations with diffusion terms," Phys. Rev.  $\bf 104$ , 563–
- <sup>12</sup>P. T. Callaghan, A. Coy, L. C. Forde, and C. J. Rofe, "Diffusive relaxation and edge enhancment in NMR microscopy," J. Mag. Res. Ser. A 101, 347-
- <sup>13</sup>T. M. de Swiet and P. N. Sen, "Decay of nuclear magnetization by bounded diffusion in a constant field gradient," J. Chem. Phys. 100, 5597-5604 (1994).
- <sup>14</sup>T. M. de Swiet, "Diffusive edge enhancment in imaging," J. Mag. Res. Ser. B 109, 12-18 (1955).
- 15 N. Moutal, K. Demberg, D. Grebenkov, and T. A. Kuder, "Localization regime in diffusion NMR: Theory and experiments," J. Mag. Res. 305, 162–
- <sup>16</sup>J. Frahm, A. Haase, and D. Matthael, "Rapid NMR imaging of dynamic
- processes using the flash technique," Mag. Res. Med. 3, 321–327 (1986). <sup>17</sup>M. Shinnar, S. Eleff, H. Subramanian, and J. S. Leigh, "The synthesis of pulse sequences yielding arbitrary magnetization vectors," Mag. Res. Med. 12, 74-80 (1989).
- <sup>18</sup>J. Pauly, P. L. Roux, D. Nishimura, and A. Macovski, "Parameter relations for the Shinnar-Le Roux selective excitation pulse design algorithm [NMR imaging]," IEEE Transactions on Medical Imaging 10, 53-65 (1991).
- <sup>19</sup>T. D. W. Claridge, High-Resolution NMR Techniques in Organic Chemistry, 2nd ed. (Elsevier, Oxford, UK, 2009).
- <sup>2</sup>III should be noted that the selective pulse Fourier inequality differs from the traditional Fourier inequality,  $\Delta v T_p \ge 1$  where  $\Delta v$  is the standard deviation in frequency and not  $\Delta v_{\perp}$ .
- <sup>21</sup>J. Keski-Rahkonen, P. J. J. Luukko, L. Kaplan, E. J. Heller, and E. Rasanen, "Controllable quantum scars in semiconductor quantum dots," Phys. Rev.
- <sup>22</sup>J. Keski-Rahkonen, A. Ruhanen, E. Heller, and E. Rasanen, "Quantum lissajous scars," Phys. Rev. Lett. 123, 214101 (2019).

This is the author's peer reviewed, accepted manuscript. However, the online version of record will be different from this version once it has been copyedited and typeset.

PLEASE CITE THIS ARTICLE AS DOI: 10.1063/5.0090041



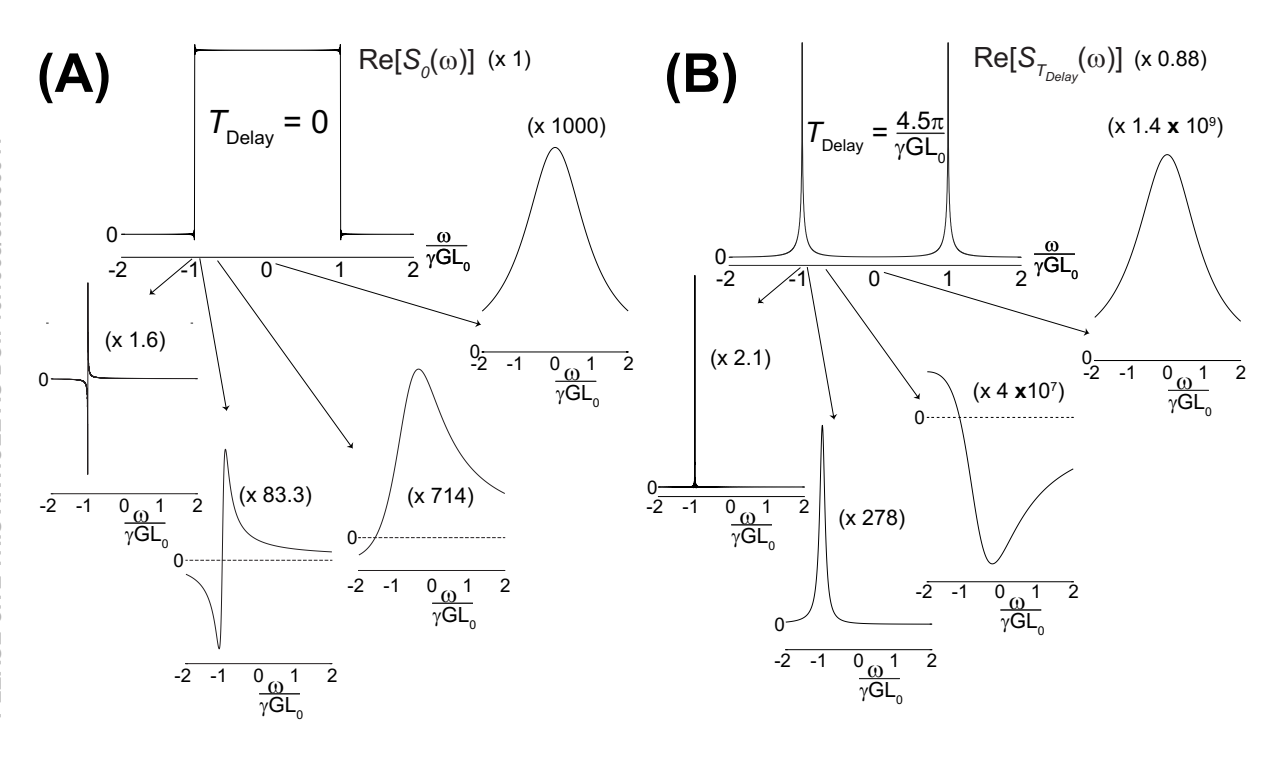


# **Applied Physics Letters**



This is the author's peer reviewed, accepted manuscript. However, the online version of record will be different from this version once it has been copyedited and typeset.

PLEASE CITE THIS ARTICLE AS DOI: 10.1063/5.0090041



# **Applied Physics Letters**



This is the author's peer reviewed, accepted manuscript. However, the online version of record will be different from this version once it has been copyedited and typeset.

PLEASE CITE THIS ARTICLE AS DOI: 10.1063/5.0090041

